Channel Estimation for MIMO System Assisted by Intelligent Reflective Surface

Gilderlan T. de Araújo, Lucas C. de P. Pessoa and André L. F. de Almeida

***Abstract*— Intelligent reflective surface (IRS) has being envisioned to be the key technology for beyond 5G or 6G systems. Due to the passive nature of the IRS, channel estimation is one of the main challenges in IRS-based communications. In addition, due to hardware constraints, a perfect reflection cannot always be achieved by the IRS. In this paper, we face the channel estimation problem in a multiple-input and multiple-output (MIMO) communication system assisted by an IRS, where a base station (BS) communicates with an user terminal (UT) via an IRS panel. We discuss two channel estimation schemes. The first is based on the least squares (LS) estimator, while the second adds an extra step based on the Khatri-Rao factorization (KRF) algorithm to achieve separate estimates of the BS-IRS and IRS-UT channels via rank-1 approximation steps. By using simplified models to capture a non-perfect IRS reflection, we numerically evaluate the performance of the two channel estimation schemes and discuss their normalized mean square error (NMSE) performance for some scenarios, including the effect of quantized IRS phase shifts and non-constant reflection amplitudes.**

***Keywords*— Intelligent reflective surface, Channel estimation, MIMO, Least Squares, Khatri-Rao factorization, PARAFAC.**

I. Introduction

The 5G technology is in the commercialization step. According to Cisco Annual Internet Report $(2018-2023)$ [1], mobile connectivity until 2023 will be over 70 percent of the global population. Moreover, the report says that over 10 percent of the devices and connections will be using 5G technology. In this context, it is necessary to investigate the limits of this technology. Several researchers have been looking at solutions for beyond 5G or even 6G technology [2], [3].

Recently, some works have discussed a new paradigm for wireless communications, which consists of smartly controlling the propagation environment by means of an Intelligent Reflective Surface (IRS) [4], [5]. Generally speaking, an IRS is a large 2D array composed of nearly passive low-cost reflecting elements designed to dynamically control the electromagnetic properties of radio-frequency waves so that the reflected signals add coherently at the intended receiver or destructively to reduce co-channel interference. An IRS can be used to increase coverage, data rates and energy efficiency in wireless communication systems [6]–[8]. It differs from conventional relaying technology since it does not require dedicated RF sources. Indeed, due to its low power consumption, energy harvesting components can be enough to supply the necessary power [9]. It is worth mentioning that [10] establishes a comparative study between IRS and relay systems where a tradeoff about the number of IRS elements and relay systems is shown. Figure 1 provides an illustration to show different scenarios where IRS can be employed in a wireless communication system.

Despite the potentials of IRS technology, several challenges must be overcome. Among them, channel estimation is a critical task in IRS-assisted wireless systems due to the passive nature and a large number of IRS elements. Research efforts have been made to better understand the channel estimation problem and develop cost-effective solutions to it. In [11], the authors formulate the channel estimation problem as a non-convex problem, and a manifold optimization is proposed to solve them. In [12], a tensor approach is employed to derive channel estimation schemes from a structured time-domain pilot pattern. In [13], compressed sensing methods are leveraged to solve the channel estimation in the context of IRS-assisted THz MIMO systems. In order to reduce the training time resources, [14] proposes an algorithm that carries out the channel estimation in three phases, where each step uses a different training time-window.

Most of the works that deals with IRS performance evaluation assume a perfect IRS reflection, i.e., the reflection amplitudes of the active IRS elements are always fixed and have a unity amplitudes. However, when considering practical aspects such as inductance, effective capacitance and resistance, and angular frequency of the incident signal, an ideal (constant) reflection amplitude cannot be guaranteed. In addition, the IRS phase shifts usually have a limited resolution due to hardware constraints. The work [15] discusses a practical model for the phase and the amplitude of the IRS-reflected signal. Also, in [16] the authors study practical effects of the electrical components over the phase and the amplitude responses.

In this paper, we take such practical amplitude and phase limitations into account in the perspective of channel estimation. More specifically, we discuss two channel estimation schemes, where the first is based on the least squares (LS) estimator, while the second adds an extra step based on the Khatri-Rao factorization algorithm to achieve separate estimates of the BS-IRS and IRS-UT channels via rank-1 approximation steps. We analyze numerically the performance of the two presented channel estimation schemes, and discuss their involved trade-

G. T. de Araújo, L. C. de P. Pessoa and A. L. F. de Almeida are with the Wireless Telecommunications Research Group (GTEL), Department of Teleinformatics Engineering (DETI), Federal University of Ceará (UFC), Fortaleza, Brazil. E-mails: gilderlan.tavares@ifce.edu.br, lucascampos@gtel.ufc.br, andre@gtel.ufc.br. This work was supported by the Ericsson Research, Sweden, and Ericsson Innovation Center, Brazil, under UFC.47 Technical Cooperation Contract Ericsson/UFC. This study was financed in part by the Coordenação de Aperfeiçoamento de Pessoal de Nível Superior - Brasil (CAPES)-Finance Code 001, and CAPES/PRINT Proc. 88887.311965/2018-00. André L. F. de Almeida like to acknowledge CNPq for its financial support under the grant 306616/2016-5.

offs, while discussing the impact of limitations on the phase and amplitude responses of the IRS on the NMSE performance of the estimated channels. In particular, our numerical results show that adding the Khatri-Rao factorization step offers a performance gain over the traditional LS channel estimator.

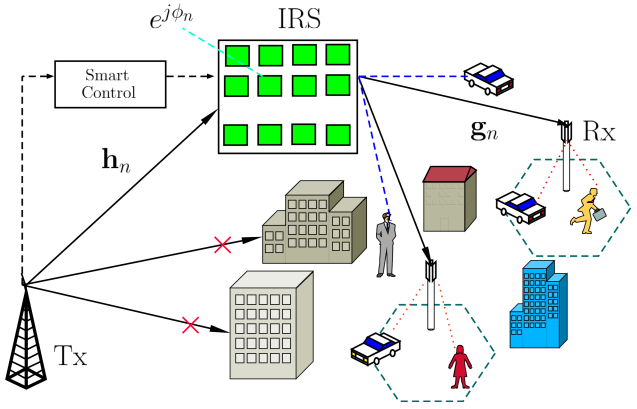

Fig. 1. Generic IRS-assisted wireless communication system.

Notation: Matrices are represented with boldface capital letters $(\mathbf{A}, \mathbf{B}, \dots)$ and vectors are denoted by boldface lowercase letters $(\mathbf{a}, \mathbf{b}, \dots)$. Tensors are symbolized by calligraphic letters $(\mathcal{A}, \mathcal{B}, \dots)$. Transpose and pseudo-inverse of a matrix $\mathbf{A}$ are denoted as $\mathbf{A}^T$ and $\mathbf{A}^\dagger$, respectively. The operator $\text{diag}(\mathbf{a})$ forms a diagonal matrix out of its vector argument, while $\odot$, $\diamond$ and $\otimes$ denote the Hadamard, Khatri-Rao and Kronecker products, respectively. $\mathbf{I}_N$ denotes the $N \times N$ identity matrix. The operator $\text{vec}(\cdot)$ vectorizes an $I \times J$ matrix argument by stacking its columns, while $\text{unvec}_{I\times J}(\cdot)$ does the opposite operation.

II. System Model

We consider a MIMO communication system assisted by an IRS. Both the transmitter and the receiver are equipped with multiple antennas. Although the terminology adopted in this paper assumes a downlink communication, where the transmitter is the base station (BS) and the receiver is the user terminal (UT), our signal model also applies to the uplink case by just inverting the roles of the transmitter and the receiver. The base station and user terminal are equipped with arrays of M and L antennas, respectively. The IRS is composed of N elements, or unit cells, capable of individually adjusting their reflection coefficients (i.e., phase shifts). The line-of-sight (LOS) path between the BS and UT is assumed to be unavailable. The system model is illustrated in Figure 2. Assuming a block-fading channel, the received signal model can be expressed as follows

$$\mathbf{y}[t] = \mathbf{G}(\mathbf{s}[t] \odot \mathbf{H}\mathbf{x}[t]) + \mathbf{n}[t], \quad t = 1, \dots, T, \tag{1}$$

or, alternatively,

$$\mathbf{y}[t] = \mathbf{G}\text{diag}(\mathbf{s}[t])\mathbf{H}\mathbf{x}[t] + \mathbf{n}[t], \tag{2}$$

where $\mathbf{x}[t] \in \mathbb{C}^{M\times 1}$ is the vector containing the transmitted pilot signals at time t, $\mathbf{s}[t] = \left[a_{1,t}e^{j\phi_{1,t}}, \dots, a_{N,t}e^{j\phi_{N,t}}\right]^T \in \mathbb{C}^{N\times 1}$ is the vector that models the phase shifts and activation

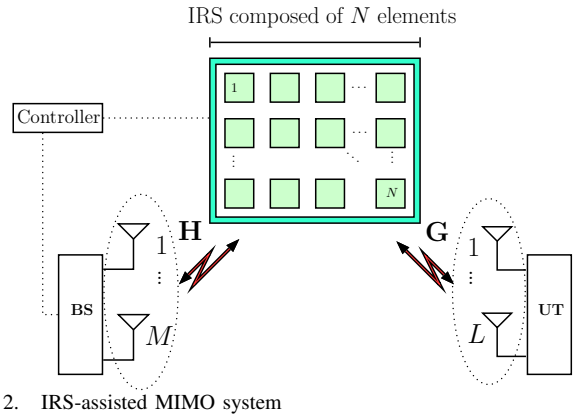

Fig. 2. IRS-assisted MIMO system

pattern of the IRS, where $\phi_{n,t} \in (0, 2\pi]$, and $a_{n,t} \in (0, 1)$ controls the amplitude of the corresponding element at time t. In practical terms, the IRS cannot design an infinity number of phases for each element due to the hardware limitations [13], [15]–[17]. Thus, considering a limited (finite) number of discrete phases is more realistic than assuming unconstrained phases. For this reason, for given ϕ_{min} and ϕ_{max}, we can uniformly distribute the phases such that they fall within a finite grid defined as

$$\mathbb{F} = \{\phi_{min}, \phi_{min} + \Delta\phi, \dots, \phi_{min} + (F-1)\Delta\phi\}, \tag{3}$$

where $\Delta\phi = \dfrac{(\phi_{max} - \phi_{min})}{F}$ and $F = 2^b$ denotes the number of discrete phase levels for b bits. It is worth mentioning that besides this phase shift constraint, the reflection amplitude is also subject to restrictions. In this paper, we investigate such an amplitude constraint by assuming $s_{n,t} \neq 1$. The matrices of uncorrelated Rayleigh fading channels $\mathbf{H} \in \mathbb{C}^{N\times M}$ and $\mathbf{G} \in \mathbb{C}^{L\times N}$ denote the BS-IRS and IRS-UT MIMO channels, respectively, while $\mathbf{n}[t] \in \mathbb{C}^{L\times 1}$ is the additive white Gaussian noise (AWGN) vector.

The channel coherence time T_s is divided into K blocks, where each block has T time slots, so that $T_s = KT$. Let us define $\mathbf{y}[k, t] \doteq y[(k-1)T + t]$ as the received signal at the t-th time slot of the k-th block, $t = 1, \dots, T$, $k = 1, \dots, K$. Likewise, denote $\mathbf{x}[k, t]$ and $\mathbf{s}[k, t]$ as the pilot signal and phase shift vectors associated with the t-th time slot of the k-th block. We propose the following structured time-domain protocol: i) the IRS phase shift vector is constant during T time slots of the k-th block and varies from block to block; ii) the pilot signals $\{\mathbf{x}[1], \dots, \mathbf{x}[T]\}$ are repeated over the K blocks. Mathematically, this means that

$$\mathbf{s}[k, t] = \mathbf{s}[k], \text{ for } t = 1, \dots, T, \tag{4}$$

$$\mathbf{x}[k, t] = \mathbf{x}[t], \text{ for } k = 1, \dots, K. \tag{5}$$

An illustration of this time-domain protocol is shown in Figure 3. Under these assumptions, the received signal model (2) can be written as

$$\mathbf{y}[k, t] = \mathbf{G}\text{diag}(\mathbf{s}[k])\mathbf{H}\mathbf{x}[t] + \mathbf{n}[k, t], \tag{6}$$

Collecting the received signals during T time slots for the k-th block in $\mathbf{Y}[k] = [\mathbf{y}[k, 1] \dots \mathbf{y}[k, T]] \in \mathbf{C}^{L\times T}$ leads to

$$\mathbf{Y}[k] = \mathbf{G}\mathbf{D}_k(\mathbf{S})\mathbf{H}\mathbf{X}^{\mathrm{T}} + \mathbf{N}[k], \tag{7}$$

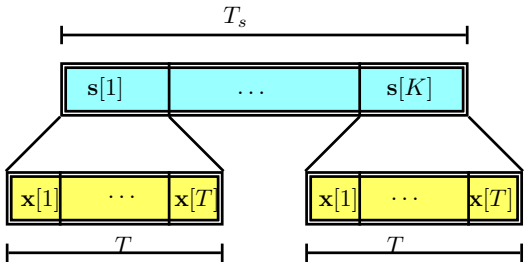

Fig. 3. Structured pilot pattern in the time domain

where $\mathbf{X} \doteq [\mathbf{x}[1], \ldots, \mathbf{x}[T]]^{\mathrm{T}} \in \mathbb{C}^{T\times M}$, $\mathbf{N} \doteq [\mathbf{n}[1], \ldots, \mathbf{n}[T]]^{\mathrm{T}} \in \mathbb{C}^{L\times T}$, $\mathbf{S} \doteq [\mathbf{s}[1], \ldots, \mathbf{s}[K]]^{\mathrm{T}} \in \mathbb{C}^{K\times N}$, and $\mathbf{D}_k(\mathbf{S}) \doteq \mathrm{diag}(\mathbf{s}[k])$ denotes a diagonal matrix holding the k-th row of the IRS phase shift matrix $\mathbf{S}$ on its main diagonal. The matrix $\mathbf{S}$ can be defined as a Hadamard product between $\mathbf{A}$ and $\mathbf{\Phi}$ whose entries are $a_{k,n}$ and $e^{j\phi_{k,n}}$, respectively.

In order to simplify the exposition of the signal model, we remove the noise term from the following developments. The noise term will be taken into account later. We can rewrite the signal part of equation (7) as

$$\mathbf{Y}[k] = \mathbf{G}\mathbf{D}_k(\mathbf{S})\mathbf{Z}^{\mathrm{T}}, \quad \mathbf{Z} \doteq \mathbf{X}\mathbf{H}^{\mathrm{T}} \in \mathbb{C}^{T\times N}. \tag{8}$$

In fact, the matrix $\mathbf{Y}[k]$ can be viewed as the k-th frontal matrix slice of a three-way tensor $\mathcal{Y} \in \mathbb{C}^{L\times T\times K}$ that follows a PARAFAC decomposition, also known as the canonical polyadic decomposition (CPD) [18]–[21].

III. Least Squares Channel estimation

In the previous section, we arrived at a received signal model that follows a PARAFAC model. Exploiting this tensor model, we present a closed-form solution consisting of a two-stage combination of the conventional LS estimation with a Khatri-Rao Factorization (KRF) method. We first write the received signal tensor $\mathcal{Y}$ using the n-mode product notation as follows

$$\mathcal{Y} \;=\; \mathcal{I}_{3,N} \times_1 \mathbf{G} \times_2 \mathbf{Z} \times_3 \mathbf{S}, \tag{9}$$

knowing that $\mathbf{Z} = \mathbf{X}\mathbf{H}^{\mathrm{T}}$, the 3-mode unfolding of the received signal tensor $\mathcal{Y}$ is given as

$$[\mathcal{Y}]_3 = \mathbf{S}\left(\mathbf{X}\mathbf{H}^{\mathrm{T}} \diamond \mathbf{G}\right)^{\mathrm{T}} \;\in\; \mathbb{C}^{K\times TL}. \tag{10}$$

Applying the property $(\mathbf{A}\otimes\mathbf{B})(\mathbf{C}\diamond\mathbf{D}) = (\mathbf{A}\mathbf{C})\diamond(\mathbf{B}\mathbf{D})$ to (10) yields

$$\begin{aligned}
[\mathcal{Y}]_3 \;&=\; \mathbf{S}\left(\mathbf{X}\mathbf{H}^{\mathrm{T}} \diamond \mathbf{G}\right)^{\mathrm{T}} && (11)\\
&=\; \mathbf{S}\left[(\mathbf{X}\otimes\mathbf{I}_L)\left(\mathbf{H}^{\mathrm{T}} \diamond \mathbf{G}\right)\right]^{\mathrm{T}} && (12)\\
&=\; \mathbf{S}\left(\mathbf{H}^{\mathrm{T}} \diamond \mathbf{G}\right)^{\mathrm{T}}(\mathbf{X}\otimes\mathbf{I}_L)^{\mathrm{T}}. && (13)
\end{aligned}$$

Defining $\mathbf{\Xi} = (\mathbf{X}\otimes\mathbf{I}_L) \in \mathbb{C}^{TL\times ML}$, equation (13) can be rewritten as

$$[\mathcal{Y}]_3 = \mathbf{S}\left(\mathbf{H}^{\mathrm{T}} \diamond \mathbf{G}\right)^{\mathrm{T}}\mathbf{\Xi}^{\mathrm{T}}. \tag{14}$$

or, equivalently,

$$[\mathcal{Y}]_3^{\mathbf{T}} = \mathbf{\Xi}\left(\mathbf{H}^{\mathrm{T}} \diamond \mathbf{G}\right)\mathbf{S}^{\mathrm{T}}. \tag{15}$$

From a noisy corrupted version of (15), a bilinear time-domain filtering is applied at the receiver by exploiting the knowledge of the IRS matrix and the pilot signal matrix. This filtering operations lead to an LS estimate of the equivalent channel as

$$\mathbf{W} \doteq \mathbf{\Xi}^{\dagger}[\mathcal{Y}]_3^{\mathrm{T}}\left(\mathbf{S}^{\mathrm{T}}\right)^{\dagger} = \left(\mathbf{H}^{\mathrm{T}} \diamond \mathbf{G}\right) + \tilde{\mathbf{N}}_3^{\mathrm{T}}, \tag{16}$$

where $\tilde{\mathbf{N}}_3 = \mathbf{\Xi}^{\dagger}[\mathcal{N}]_3^{\mathrm{T}}\left(\mathbf{S}^{\mathrm{T}}\right)^{\dagger}$ is the filtered noise term. Note that $\mathbf{W} \in \mathbb{C}^{ML\times N}$ is a noisy version of the (Khatri-Rao structured) *virtual MIMO channel* that models the IRS-assisted MIMO transmission. Exploiting such a Khatri-Rao structure, in the next section we present an algorithm to provide separate estimates of the BS-IRS and IRS-UT channel matrices. As will be clear later, solving the equivalent channel estimation problem via KRF algorithm will provides an improved accuracy compared to the LS scheme thanks to the denoising achieved by the multiple rank-1 matrix factorization steps.

IV. KRF-based channel estimation

In the previous section, we have presented the conventional LS-based channel estimation method, which yields an estimate of the equivalent BS-IRS-UT channel matrix that has a Khatri-Rao product structure. Starting from the LS solution in equation (16), we propose to estimate $\mathbf{H}$ and $\mathbf{G}$ by minimizing the following cost function

$$\min_{\mathbf{H},\mathbf{G}} \left\|\mathbf{W} - \mathbf{H}^{T} \diamond \mathbf{G}\right\|_F^2 \tag{17}$$

An efficient solution to this problem is given by the Khatri-Rao factorization (KRF) algorithm [22], [23]. The problem (17) can be interpreted as finding estimates of $\mathbf{H}$ and $\mathbf{G}$ that solve a set of rank-1 matrix approximation problems, i.e.,

$$(\hat{\mathbf{H}}, \hat{\mathbf{G}}) = \underset{\{\mathbf{h}_n\},\{\mathbf{g}_n\}}{\arg\min} \sum_{n=1}^{N} \left\|\tilde{\mathbf{W}}_n - \mathbf{g}_n\mathbf{h}_n^{\mathrm{T}}\right\|_F^2, \tag{18}$$

where $\tilde{\mathbf{W}}_n \doteq \mathrm{unvec}_{L\times M}(\mathbf{w}_n) \in \mathbf{C}^{L\times M}$, while $\mathbf{g}_n \in \mathbf{C}^{L\times 1}$ and $\mathbf{h}_n^{\mathrm{T}} \in \mathbf{C}^{1\times M}$ are the n-th column and n-th row of $\mathbf{G}$ and $\mathbf{H}$, respectively. The estimates of $\mathbf{g}_n$ and $\mathbf{h}_n$ in (18) can be obtained from the dominant left and right singular vectors of $\tilde{\mathbf{W}}_n$, respectively, for $n = 1, \ldots, N$. Hence, our channel estimation problem translates into solving N rank-1 matrix approximation subproblems, for which several efficient solutions exist in the literature, such as the well-known power method [24]. A summary of the algorithm, herein referred to as KRF, is given in Algorithm 1, where t-SVD denotes a truncated SVD that returns the dominant singular vectors and associated singular value.

The estimates $\hat{\mathbf{G}}$ and $\hat{\mathbf{H}}$ are affected by scaling ambiguities. More specifically, the rows of $\hat{\mathbf{H}}$ and the columns of $\hat{\mathbf{G}}$ are affected by unknown scaling factors that compensate each other, i.e., $\hat{\mathbf{H}} = \mathbf{\Delta}_H\mathbf{H}$ and $\hat{\mathbf{G}} = \mathbf{G}\mathbf{\Delta}_G$. Note, however, that such a scaling ambiguity is automatically eliminated in the estimate of the cascaded channel, i.e, $\mathbf{\Delta}_G\mathbf{\Delta}_H = \mathbf{I}_N$.

Design requirements and computational cost: The KRF method (Algorithm 1) has a bilinear filtering step as shown in (16), requiring that $\mathbf{S}$ and $\mathbf{\Xi}$ be semi-unitary (or column-orthogonal) matrices, which implies $K \geq N$ and $T \geq M$. Regarding the computational cost, the extra cost added by the KRF algorithm corresponds to that of N rank-1 approximation routines. The computational cost of the KRF algorithm is approximately equal to $\mathcal{O}(MLN)$.

Algorithm 1: Khatri-Rao Factorization (KRF)

Procedure
begin
Bilinear filtering of $[\mathcal{Y}]_3$:
$\mathbf{W}^{\mathrm{T}} \longleftarrow \mathbf{S}^{\dagger}[\mathcal{Y}]_3 \left(\mathbf{\Xi}^{\mathrm{T}}\right)^{\dagger}$
for $n = 1, \ldots, N$ **do**
$\tilde{\mathbf{W}}_n \longleftarrow \text{unvec}_{L\times M}(\mathbf{w}_n)$
$(\mathbf{u}_1, \sigma_1, \mathbf{v}_1) \longleftarrow \text{t-SVD}(\tilde{\mathbf{W}}_n)$
$\hat{\mathbf{h}}_n \longleftarrow \sqrt{\sigma_1}\mathbf{v}_1^*$
$\hat{\mathbf{g}}_n \longleftarrow \sqrt{\sigma_1}\mathbf{u}_1$
end
Reconstruct $\hat{\mathbf{H}}$ *and* $\hat{\mathbf{G}}$:
$\hat{\mathbf{H}} \longleftarrow \left[\hat{\mathbf{h}}_1, \ldots, \hat{\mathbf{h}}_N\right]^T$
$\hat{\mathbf{G}} \longleftarrow [\hat{\mathbf{g}}_1, \ldots, \hat{\mathbf{g}}_N]$

V. Numerical Results

In this section, some numerical results are presented. The channel estimation accuracy is evaluated in terms of the normalized mean square error (NMSE) given by

$$\text{NMSE}(\hat{\mathbf{H}}) = \frac{1}{R}\sum_{r=1}^{R}\left(\frac{\|\mathbf{H}^{(r)} - \hat{\mathbf{H}}^{(r)}\|_F^2}{\|\mathbf{H}^{(r)}\|_F^2}\right), \qquad (19)$$

where $\hat{\mathbf{H}}^{(r)}$ is the BS-IRS channel estimated at the r-th run, and R denotes the number of Monte Carlo runs. The same definition applies to the estimated IRS-UT channel. The SNR (in dB) is defined as $\text{SNR} = 10\log_{10}\left(\|[\mathcal{Y}]_3\|_F^2/\|[\mathcal{N}]_3\|_F^2\right)$. At each run, the channel matrices $\mathbf{H}$ and $\mathbf{G}$ and noise term are drawn from an i.i.d. complex-valued Gaussian distribution. To evaluate the impact of the limited resolution of the IRS phases on the channel estimation accuracy, we assume that the IRS phase shift matrix $\mathbf{S} \in \mathbb{R}^{K\times N}$ has random entries to amplitudes lying between 0 and 1, which are drawn from a uniform distribution at each run. Note that optimizing the reflection amplitudes it is out of the scope of this work, since deal with the channel estimation problem and optimization of the IRS phases requires the knowledge of the BS-IRS and IRS-UT channels.

First, in (2) we evaluate the impact of the amplitude constraint, i.e, $0 < a_{n,t} < 1$, on the estimation of the equivalent and individual channels. Here, the phase shift matrix is designed as a truncated DFT matrix and no constraints on the resolution of the phases are imposed. The results are depicted in Figures 4-5. When the LS solution is considered, the equivalent channel $\left(\mathbf{H}^{\mathrm{T}} \diamond \mathbf{G}\right)$ is estimated directly from equation (15). On the other hand, when considering the KRF algorithm, the equivalent channel is reconstructed from the separate estimates of the channels $\mathbf{H}$ and $\mathbf{G}$. As expected, the performance it is better when the IRS matrix has constant amplitudes (i.e. $a_{k,n} = 1, \forall\ k, n$). An SNR loss of approximately 1.5dB can be observed for the whole SNR range when considering the nonideal amplitude model. In particular, in Figure 4, we can also observe that the KRF algorithm outperforms the LS algorithm. The SNR gap between both methods is approximately 3dB, which means that the KRF algorithm effectively filters out the residual noise that affect the LS estimate by providing an NMSE performance enhancement in comparison to the single-stage LS estimation of the equivalent channel. Indeed, the KRF algorithm adds an extra rank-1 matrix approximation step by reshaping the effective $ML \times N$ "Khatri-Rao"channel in the form of N matrices of dimension $M \times L$. This rank-1 approximation achieves an additional noise rejection, which translates into an improved channel estimation accuracy. Figure 5 shows the impact of the nonideal IRS amplitude responses on the estimation of the cascaded channel. We define the cascaded channel as $\hat{\mathbf{H}}_C \doteq \hat{\mathbf{G}}\hat{\mathbf{H}}$. We can also note a degradation of around 1.5dB, following the results of the previous figure.

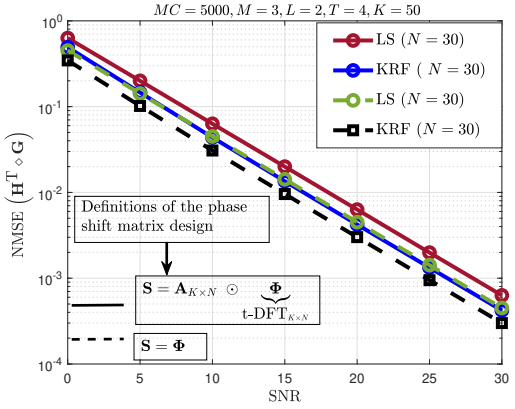

Fig. 4. NMSE of the estimated equivalent channels $\hat{\mathbf{H}}^{\mathrm{T}} \diamond \hat{\mathbf{G}}$.

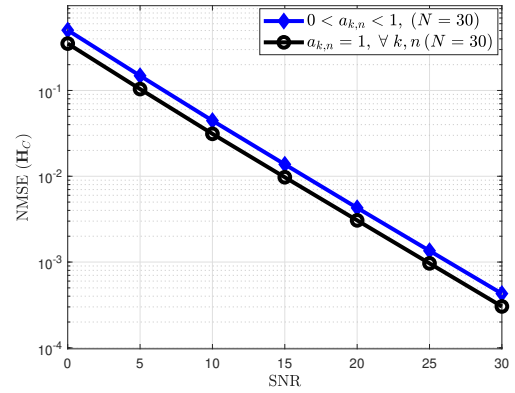

Fig. 5. NMSE of the estimated cascaded channel $\hat{\mathbf{H}}_C = \hat{\mathbf{G}}\hat{\mathbf{H}}$.

Next, supposing no amplitude fluctuations on the IRS reflection matrix, we add the assumption of limited resolution phase shifts, and evaluate its impact on the channel estimation accuracy. In this case, the IRS has a limited number of available phases that belong to finite set $\mathbb{F}$ defined in (3). The results are depicted in Figure 6 (for the LS method) and in Figure 7 (for the KRF method). We compare two limited resolution design approaches. The first approach corresponds to the quantized DFT grid according to [17], while the second corresponds to a binary design, where the IRS matrix is designed as a truncated Hadamard matrix. For the quantized DFT design, we assume $b = 4$ bits. For the Hadamard design,

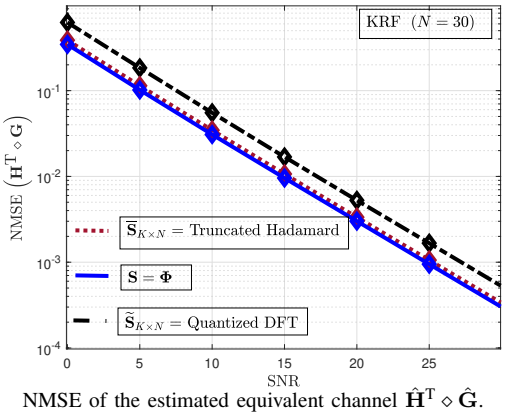

Fig. 6. NMSE of the estimated equivalent channel $\hat{\mathbf{H}}^{\mathrm{T}} \diamond \hat{\mathbf{G}}$.

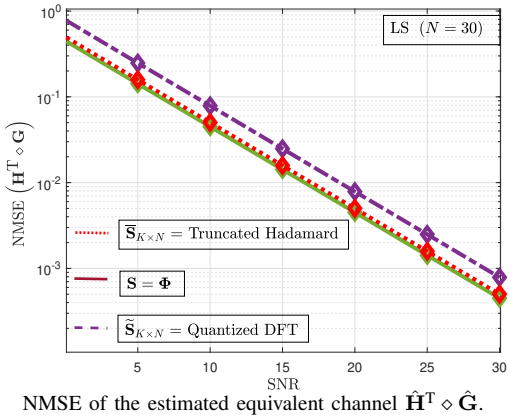

Fig. 7. NMSE of the estimated equivalent channel $\hat{\mathbf{H}}^{\mathrm{T}} \diamond \hat{\mathbf{G}}$.

we necessarily have $b = 1$ bit, i.e., the IRS elements only assume two states given by $\{1, -1\}$. First, we can observe a degradation on the channel estimation accuracy when the quantized DFT design is used, while the binary Hadamard design is very close to the ideal case where no constraints are imposed on the phase shifts.

VI. Conclusion

In this paper, we have discussed different solutions to solve the channel estimation problem in an MIMO IRS-assisted system. We found out that the proposed KRF algorithm provides an improvement on the NMSE of the estimated channels in comparison to the classical LS estimator. Such a performance gain comes from the efficient exploitation of the Khatri-Rao structure of the equivalent channel. We have also evaluated the impact of nonideal IRS amplitude and phase shift responses. A slight degradation was observed when the phase shifts are quantized in a DFT grid. We also noted that the Hadamard design provides more accurate channel estimates than the quantized DFT one, while requiring less bits. This observation has a practical impact, since the IRS reflection coefficients are usually conveyed from the BS to the IRS through a low-rate limited feedback control channel. A perspective of this work is the extension of the KRF channel estimation method to the multiuser case. The use of more realistic parametric (circuit-based) phase shift models for the IRS should also be considered and their impact on the channel estimation performance should be evaluated.

References

[1] "Cisco annual internet report (2018–2023)," White paper Cisco public, Tech. Rep.

[2] C. H. et al., "Holographic MIMO surfaces for 6G wireless networks: Opportunities, challenges, and trends," Apr 2020, https://arxiv.org/pdf/1911.12296.pdf.

[3] E. Basar, "Reconfigurable intelligent surface-based index modulation: A new beyond MIMO paradigm for 6G," Aug 2019, https://arxiv.org/abs/1904.06704.

[4] M. D. R. et al, "Smart radio environments empowered by reconfigurable intelligent surfaces: How it works, state of research, and road ahead," Aug 2020, https://arxiv.org/pdf/2004.09352.pdf.

[5] L. D. et al., "Reconfigurable intelligent surface-based wireless communications: Antenna design, prototyping, and experimental results," *IEEE Access*, vol. 8, 2020.

[6] V. C. Thirumavalavan and T. S. Jayaraman, "BER analysis of reconfigurable intelligent surface assisted downlink power domain NOMA system," in *2020 International Conference on COMmunication Systems & NETworkS (COMSNETS)*, Bengaluru, India, 2020.

[7] M. Zeng, X. Li, G. Li, W. Hao, and O. A. Dobre, "Sum rate maximization for IRS-assisted uplink NOMA," Apr 2020, https://arxiv.org/pdf/2004.10791v1.pdf.

[8] Y. Liu, E. Liu, and R. Wang, "Energy efficiency analysis of intelligent reflecting surface system with hardware impairments," Apr 2020, https://arxiv.org/pdf/2004.09804v1.pdf.

[9] A. S. de Sena et al., "What role do intelligent reflecting surfaces play in non-orthogonal multiple access?" 2020, https://doi.org/10.36227/techrxiv.11791050.v1.

[10] E. Bjornson, O. Ozdogan, and E. G. Larsson, "Intelligent reflecting surface versus decode-and-forward: How large surfaces are needed to beat relaying?" *IEEE Wireless Communications Letters*, vol. 9, no. 2, pp. 244–248, Feb 2020.

[11] T. Lin, X. Yu, Y. Zhu, and R. Schober, "Channel estimation for intelligent reflecting surface-assisted millimeter wave MIMO systems," may 2020, https://arxiv.org/abs/2005.04720.

[12] G. de Araújo and A. L. F. de Almeida, "PARAFAC-based channel estimation for intelligent reflective surface assisted MIMO system," in *in 11th IEEE Sensor Array and Multichannel Signal Processing Workshop (SAM 2020)*, Hangzhou, China, Jun 2020.

[13] X. M. et al., "Joint channel estimation and data rate maximization for intelligent reflecting surface assisted terahertz MIMO communication systems," *IEEE Access*, vol. 8, pp. 99 565–99 581, 2020.

[14] Z. Wang, L. Liu, and S. Cui, "Channel estimation for intelligent reflecting surface assisted multiuser communications," in *IEEE Wireless Communications and Networking Conference (WCNC)*, 2020.

[15] S. Abeywickrama, R. Zhang, and C. Yuen, "Intelligent reflecting surface: Practical phase shift model and beamforming optimization," Feb 2020, https://arxiv.org/pdf/1907.06002v4.pdf.

[16] W. Cai, H. Li, M. Li, and Q. Liu, "Practical modeling and beamforming for intelligent reflecting surface aided wideband systems," *IEEE Communications Letters*, Apr 2020.

[17] C. You, B. Zheng, and R. Zhang, "Channel estimation and passive beamforming for intelligent reflecting surface: Discrete phase shift and progressive refinement," Mar 2020, https://arxiv.org/pdf/1912.10646v2.pdf.

[18] T. G. Kolda and B. W. Bader, "Tensor decompositions and applications," *SIAM Review*, vol. 51, no. 3, pp. 455–500, September 2009.

[19] F. L. Hitchcock, "The expression of a tensor or a polyadic as a sum of products," *Journal of Mathematical Physics*, vol. 6, no. 1, pp. 164–189, 1927.

[20] J. D. Carroll and J.-J. Chang, "Analysis of individual differences in multidimensional scaling via an n-way generalization of "Eckart–Young" decomposition," *Psychometrika*, vol. 35, no. 3, pp. 283–319, 1970.

[21] R. A. Harshman, "Foundations of the PARAFAC procedure: models and conditions for an "explanatory" multi-modal factor analysis," *UCLA Working Papers in Phonetics*, vol. 16, no. 1, pp. 84–84, 1970.

[22] A. Y. Kibangou and G. Favier, "Non-iterative solution for PARAFAC with a toeplitz matrix factor," in *2009 17th European Signal Processing Conference*, Aug 2009, pp. 691–695.

[23] F. Roemer and M. Haardt, "Tensor-based channel estimation and iterative refinements for two-way relaying with multiple antennas and spatial reuse," *IEEE Transactions on Signal Processing*, vol. 58, no. 11, pp. 5720–5735, Nov 2010.

[24] G. H. Golub and C. F. V. Loan, *Matrix Computations*, 4th ed. John Hopkins University Press, 2013.